J Mater Sci (2022) 57:467–476

Electronic materials

Pores in p-type GaN by annealing under nitrogen atmosphere: formation and photodetector

Rongrong Chen[1], Jie Liu[1], Bo Feng[1], Hongyan Zhu[1], Di Wang[1], Caina Luan[1], Jin Ma[1], Lei Zhang[2], and Hongdi Xiao[1,*]

[1] School of Microelectronics, Shandong University, Jinan 250101, People's Republic of China
[2] State Key Lab of Crystal Materials, Shandong University, Jinan 250100, People's Republic of China

Received: 3 August 2021
Accepted: 12 October 2021
Published online: 3 January 2022

ABSTRACT

Mg-doped p-GaN, which cannot be etched and porosified by wet etching, is annealed in a N_2 environment to fabricate porous p-GaN for the first time. In the annealing temperature range of 900–1150 °C, the pore size and pore density increase with the annealing temperature rising. The porous p-GaN with a V-shape pore structure obtained at 1050 °C presents the best crystal quality. We demonstrate that the formation of porous structures is largely due to the decomposition of GaN molecules located at the defects in the p-GaN epitaxial film. Porous p-GaN epitaxial wafers can be used to prepare violet light photodetectors. Compared with the as-grown sample, the porous GaN obtained at 1050 °C exhibits faster carrier mobility, higher light response speed, lower surface state density and similar visible light transmittance. Our work will promote the development of porous p-type GaN materials.

Introduction

As a common third-generation semiconductor material, GaN has excellent optical, electrical and chemical properties such as high carrier mobility, wide direct band gap (3.4 eV), high breakdown voltage (3.3 MV/cm), high chemical and thermal stability, and high thermal conductivity (1.3 W/(cm·K)) [1–4]. These excellent characteristics make GaN presents a wide range of application prospects in light-emitting devices (e.g., blue and green light-emitting diodes, blue lasers, ultraviolet detectors) and power electronic devices (e.g., heterojunction field effect transistors)[2, 5–7]. Compared to GaN epitaxial films, porous GaN obtained by etching has many advantages such as low defect density, large specific surface area and high photoelectric performance [1, 3, 8, 9]. Therefore, porous GaN can be applied in many fields such as crystal growth, water splitting, light-emitting diodes (LEDs) and energy storage [1, 10, 11].

So far, the methods for preparing porous GaN materials included dry etching and wet etching. Dry etching includes plasma etching, reactive ion etching

Handling Editor: Kevin Jones.

Address correspondence to E-mail: hdxiao@sdu.edu.cn

https://doi.org/10.1007/s10853-021-06632-4

and laser ablation. However, issues such as yield and cost make such a process still somewhat cumbersome [12–14]. Wet etching can be divided into chemical etching, electrochemical (EC) etching and photo-assisted electrochemical (PEC) etching [15, 16], which has several advantages over dry etching such as low stress, high yield, and low cost [17]. The etching mechanism is that GaN is oxidized at the defects, and then the corresponding oxide is dissolved in the etching solution (e.g., HF acid and oxalic acid) [18]. For p-GaN, however, the Fermi energy level is close to the position of the valence band, and the ionization energy required by its electrons is much greater than that of n-GaN, so it is difficult to oxidize it through electrochemical methods [19]. Therefore, it is absolutely necessary to find a high yield and lost cost method that can replace dry etching to prepare porous p-GaN.

In this paper, we explore a novel method for porosizing p-type GaN epitaxial films. The thermal annealing in N_2 ambient can lead to formation of porous p-GaN [20]. Compared with the as-grown GaN epitaxial wafer, the porous p-GaN film fabricated at 1050 °C has better crystalline quality, higher carrier mobility and similar visible light transmittance. To study the possible applications, the p-type porous GaN was made into a metal–semiconductor-metal photodetector, which has higher photoelectric response effect than the as-grown GaN detector.

Experimental details

Mg doping p-GaN(0001) films with a thickness of about 2 μm and a doping concentration of 1×10^{18} cm^{-3} are deposited on c-face sapphire (double-sided polishing and single-sided polishing) substrates by metal organic chemical vapor deposition (MOCVD). The as-grown samples are placed into tube furnace for annealing at different temperatures (e.g., 900, 1000, 1050, 1100 and 1150 °C) for 1 h under an atmosphere of high purity N_2 (5 N) (0.6 NL/min). Subsequently, the annealed samples are immersed in a boiling saturated solution of NaOH for 30 min, to reduce possible oxidation in the annealed samples. Finally, photodetectors are fabricated by using that Ti film and gold film with a thickness of 5 nm and 40 nm were grown on the GaN film before and after the annealing by a thermal evaporation method, respectively. The patterns are 250 μm-wide and 5.2 mm-long with a 100 μm wide inter-finger spacing.

The surface morphology of samples is observed by scanning electron microscope (SEM, Nova Nano SEM 450), while the high-resolution X-ray diffraction (HRXRD, Smartlab3kW) was applied to assess the lattice quality of the samples. The room-temperature Raman spectra of the samples were measured to assess the in-plane stress before and after annealing. The optical transmittance of the samples grown on the double-sided polished sapphire substrates was measured by a TU-1901 double-beam UV–Vis NIR spectrophotometer to prove the difference in optical properties, whereas the carrier concentration, mobility and resistivity of the samples before and after annealing at 1050 °C are determined by Hall test (semishare X1). The elemental composition of the sample surface was evaluated by X-ray photoelectron spectroscopy (XPS, Thermo ESCALAB 250XI). The time response measurements of photodetectors were carried out under 405 nm violet light illumination at an applied bias of 5 V.

Results and discussion

Figure 1 shows the top-view SEM images of the p-GaN(0001) samples within the temperature range of 900–1150 °C and the photographs of corresponding GaN samples. It can be observed that the annealing leads to the formation of V-shape pores which are defined by the six (10 $\bar{1}$1) planes. This is because the structure has the lowest surface energy in hexagonal wurtzite structure [21]. The pore size and density of the samples increase with the annealing temperature rising. When the temperature is or exceeds 1100 °C, the pores will begin to overlap, and pore size increases with the annealing temperature rising. The insets display the photographs of corresponding GaN samples under room light illumination and the transmittance of card printed with a logo. The logo can be clearly observed through the annealed samples at 900–1050 °C, meaning that the annealing is the uniform porosification process across the entire epitaxial wafer. Although the smooth surface of samples obtained at 1100 and 1150 °C is observed by using the naked eye, the films are opaque, which should be contributed to scattering of light due to the existence of a large number of pores.

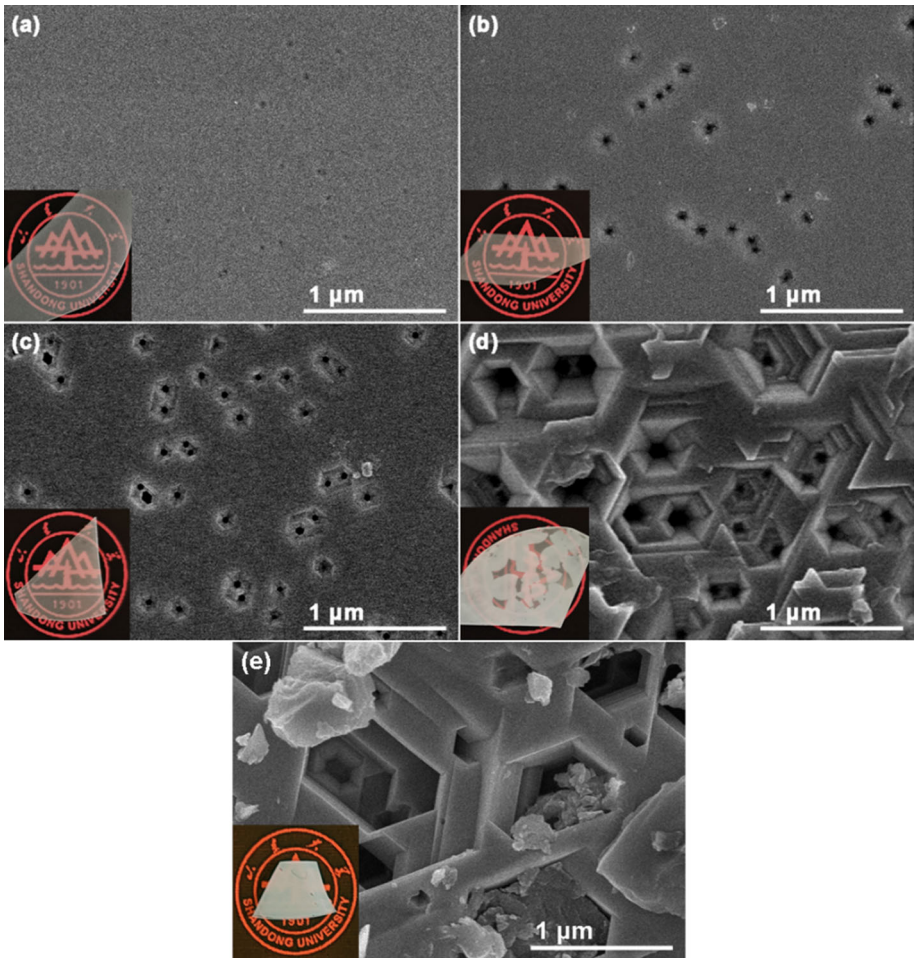

Figure 1 Top-view SEM images of p-GaN thin films annealed at **a** 900, **b** 1000, **c** 1050, **d** 1100 and **e** 1150 °C. The insets are photographs of annealed GaN samples on a card with the Shandong University Logo.

When the annealing temperatures are 1000 and 1050 °C, the pore density is 3.6×10^8 and 7.1×10^8 cm^{-2}, respectively. These values are within the reported range of threading dislocation density (10^7–10^9 cm^{-2}) [22]. It has been known that for GaN grown on sapphire substrates, most threading dislocations are parallel to the growth direction (i.e., the c-axis) [23], which is in agreement with the growth direction of V-shape pores (Fig. 2 (a)), probably indicating that the V-shape pores should be related to the threading dislocations [24, 25]. Because the lattice atoms at the defect positions have worse stability than those at other positions, the lattice molecular in the 'defect' positions are decomposed and form metal Ga [20, 24]. The corresponding chemical equation is as follows [26]:

$$2GaN(s) \rightarrow Ga(l) + N_2(g) + Ga(g).$$

Under the high temperature of more than 900 °C, the formed Ga nanodroplets are evaporated, leading to V-shape pores along the [000 $\bar{1}$] direction. When the annealing temperature is above 1100 °C, the decomposition of GaN molecules will occur across the entire GaN epitaxial wafer, resulting in formation of an opaque GaN epitaxial wafer (see the insets in Fig. 1(d) and Fig. 1(e)).

Figure 2(b) summarizes the phase diagram of the observed morphology and optical properties, which is related to annealing temperature and time. Here, the SEM images which vary with the annealing time are not provided. The phase diagram consists of mainly porous region which is opaque, porous and nonporous regions (these three regions are delineated by solid lines as a visual guide). In the porous region, the annealing temperature and time have a profound effect on the pore morphology, as shown in Fig. 1. The pore size and density increase with the annealing temperature and time rising.

To investigate the porous p-type GaN quality, the structural, optical, and electrical properties are analyzed in turn. The XRD ω-rocking curve and

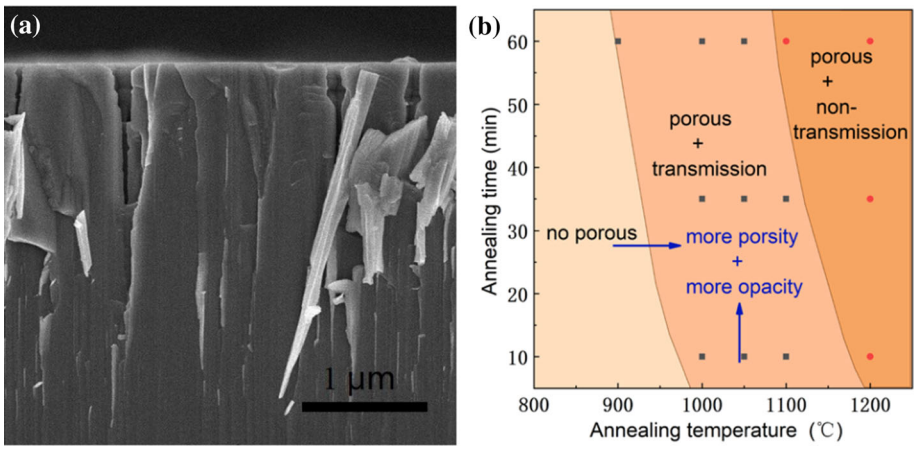

Figure 2 **a** Cross-sectional SEM images of porous p-GaN thin film annealed at 1050 °C, **b** Different annealing characteristics related to the annealing time and temperature of GaN. Three regions are defined: no porous, porous and transparent, porous and non-transparent regions.

corresponding FWHM of (0002) symmetry planes of the GaN films annealed under the different temperatures are depicted in Fig. 3. The ω-rocking curves of the GaN samples before and after the annealing do not present significant change (Fig. 3(a)), indicating that the GaN epitaxial films still have single crystal characteristics after the annealing. However, the FWHMs of the peaks narrow first and then widen with the increasing of the annealing temperature (Fig. 3(b)), meaning that the annealing can lead to improvement of GaN crystal quality in the temperature range from 900–1050 °C. The improvement could be contributable to the decrease in native defects inside the films and/or stress relaxation [17, 24]. In addition, the annealing temperature above 1100 °C will severely damage the film structure as shown in Fig. 1(d) and Fig. 1(e), leading to a significant deterioration of the crystal lattice quality of the films [27].

Figure 4 displays the room-temperature Raman spectra of the samples annealed at the different temperatures. A strong E_2 (high) peak and a weak A_1 (TO) peak are observed at 570 and 735 cm^{-1} in all samples, respectively, which meets the Raman selection rules for wurtzite GaN [28]. Although there are a lot of pores in the films, the E_2 peaks do not present significant red shift, i.e., the annealed films do not have obvious stress relaxation [29], which should be related to the sparse pores (Figs. 1 and 2(a)). The E_1 (TO) peak emerges in the spectra of the samples annealed at 1050 and 1100 °C, which should be ascribed to the increased scattering of the non-planar (e.g., pore wall) of porous GaN structures [30]. Therefore, the improvement of GaN crystal quality in Fig. 3 should be attributed to decrease in the defects rather than the stress relaxation after the annealing.

The insets in Fig. 1 only qualitatively explain the transmission characteristics of the annealed samples. To quantify the transmittance of annealed samples, the GaN films were grown double-sided polished sapphire substrates. Figure 5 shows the optical transmittance of GaN epitaxial wafers before and after the annealing. It can be seen from this figure that the optical transmittance of the 1050 °C-annealed sample can be almost consistent with that of the as-grown sample. When the temperature reaches

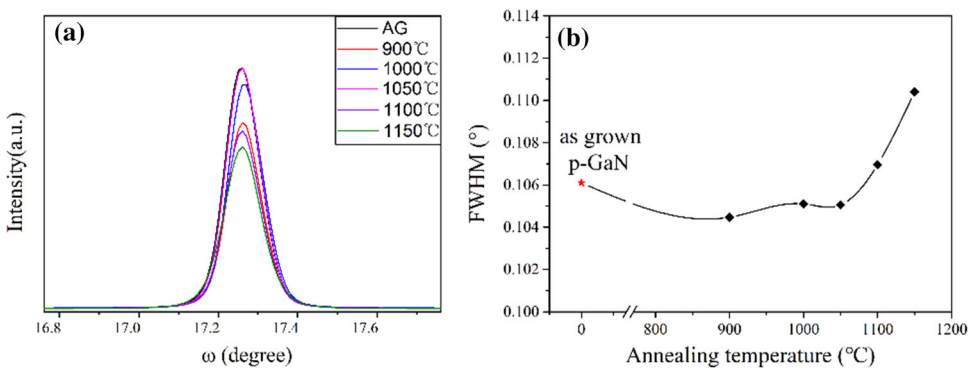

Figure 3 XRD ω-rocking curve and corresponding FWHM of (0002) symmetry planes of the GaN films treated under different annealing temperatures.

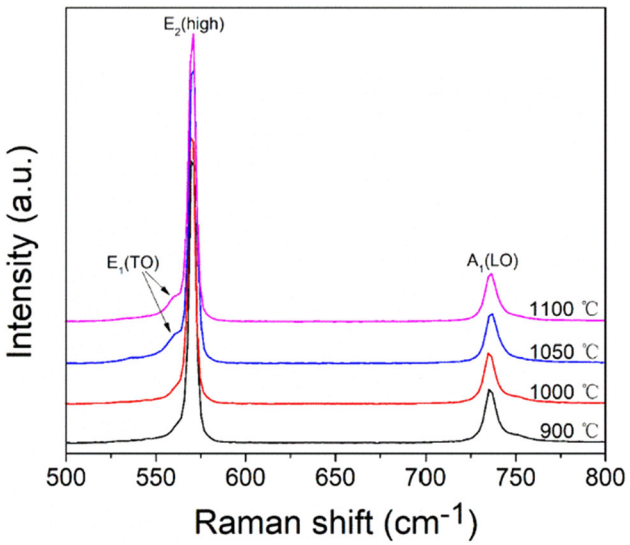

Figure 4 Raman spectra of the as-grow film and annealed at 900, 1000, 1050 and 1100 °C.

1100 °C, however, the optical transmittance decreases significantly, which is blamed to the surface structure that is damaged severely under the high anneal temperature, resulting in a significant increase in diffuse scattering [31].

The Hall test is performed to assess the changes in electrical properties before and after the annealing. The carrier concentration, mobility and resistivity of the samples before and after the annealing at 1050 °C are exhibited in Table 1. Compared to the as-grown sample, the carrier concentration of the annealed sample decreases slightly, while the carrier mobility and resistivity increase slightly. The reduction in the carrier concentration could be due to the

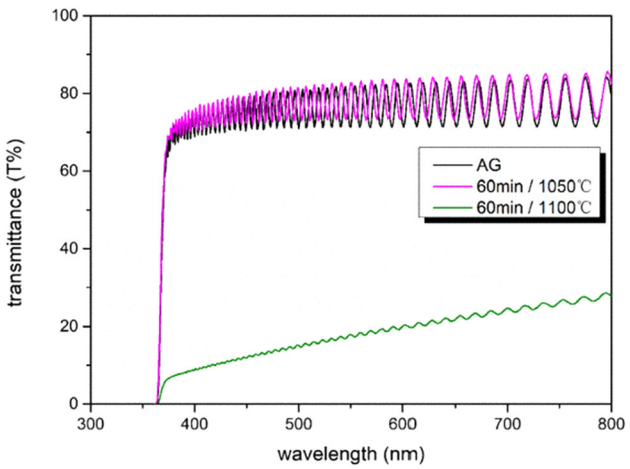

Figure 5 The optical transmittance of the annealed p-GaN wafer under the different temperatures.

decomposition of GaN region with the local high carrier concentration [18]. The increase in the carrier mobility should be related to decrease in the carrier concentration and defects. The decrease in carrier concentration leads to decrease in the scattering between free carriers, while the decrease in the defects caused by the annealing results in decrease in the scattering of lattice defects [32–35]. However, the effect of increased mobility is not enough to offset the effect of reduced carrier concentration on resistivity, so the resistivity of the annealed sample increases [36].

Figure 6 depicts the XPS scan result of the GaN thin films before and after the annealing at 1050 °C. The core peaks of the charges have been corrected by carbon peak. It can observed from Fig. 6(a) that the two samples present a O 1 s peak located at ~ 531.5 eV, mainly resulting from the adsorption of oxygen-containing pollutants on the sample [37]. Compared to the as-grown sample, the O 1 s peak of the annealed sample is stronger, which is due to larger specific surface area of porous GaN.

The XPS fine spectra of N 1 s with Ga Auger electron spectroscopy (AES) and Ga 3d of the as-grown and annealed samples are depicted in Fig. 6 (b) and Fig. 6 (c), respectively. Figure 6(b) shows that the N 1 s peaks of the as-grown and annealed GaN are centered at 395.98 and 395.78 eV, whereas the corresponding Ga 3d core lines are located at a binding energy of 18.87 and 18.17 eV (see Fig. 6(c)), respectively. These red shifts of 0.2 and 0.7 eV indicate the decrease in the number of Ga-N bonds, i.e., the number of dangling bonds in the surface region of the porous p-GaN increases, which is in agreement with Mg doped p-GaN [38]. In addition, the FWHM values of the Ga 3d and N 1 s core level peaks for the annealed sample are 1.48 and 1.2 eV, respectively, which are much smaller than those (1.60 and 1.45 eV) of the as-grown sample. These results indicate that the annealing can lead to decrease in the surface state density of the sample [39], meaning that the annealed GaN sample can create better Ohmic contacts than the as-grown p-GaN.

To investigate the possible application of porous p-GaN, the samples before and after the annealing were used to fabricate metal–semiconductor-metal photodetectors. The schematic diagram of the porous p-GaN photodetector is shown in Fig. 7 (a). Due to formation of the Schottky-type contact at the interface of the Ti and GaN, the current of the detectors keeps

Table 1 Carrier concentration, carrier mobility and resistivity of the GaN samples before and after the annealing at 1050 °C for 1 h

Sample	Carrier concentration (cm^{-3})	Carrier mobility ($cm^2 \cdot V^{-1} \cdot S^{-1}$)	Resistivity ($\Omega \cdot cm$)
As-grown	2.85×10^{17}	2.26×10^{2}	9.7×10^{-2}
Annealed	1.45×10^{17}	2.68×10^{2}	1.6×10^{-1}

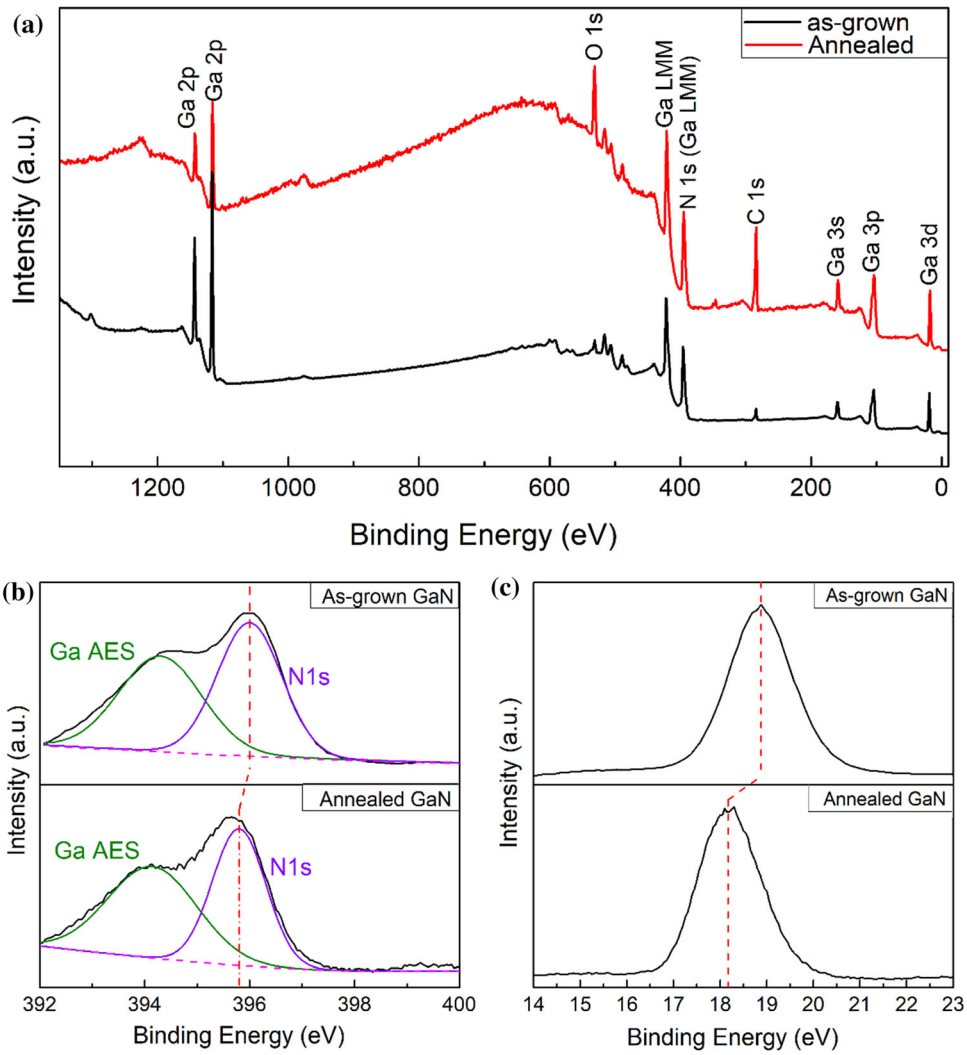

Figure 6 XPS spectra from as-grown-GaN and the sample annealed at 1050 °C for 1 h. **a** survey, **b** N 1 s and **c** Ga 3d.

a small state under dark conditions. When the devices are irradiated, the high-energy photons excite the GaN layer and generate electron–hole pairs. Subsequently, the photo-generated electrons and holes in the depletion region are separated and drift to the positive and negative electrodes under an applied bias, respectively, leading to the formation of photocurrent. The time-dependent photo responses of the photodetectors under 405 nm are display in Fig. 7 (b) and Table 2. The rise (τ_r) and fall (τ_d) times are defined as the time for the current to rise to 90% of the maximum value and the current to fall to 10% of the maximum value, respectively, whereas the on/off ratio refers to the ratio of photocurrent to dark current [40]. The photo-response of detectors at 405 nm (3.06 eV) is less than the band gap (3.4 eV) of GaN, which is due to the impurity band to widen caused by Mg doped and enter the valence band to form a band tail, resulting in a narrower band gap of the sample (Fig. 7(c)) [41].

Compared with the S_1 photodetector, the S_2 and S_3 detectors show excellent characteristic, in terms of response speed and switching ratio (see Table 2), suggesting that the GaN films after the annealing

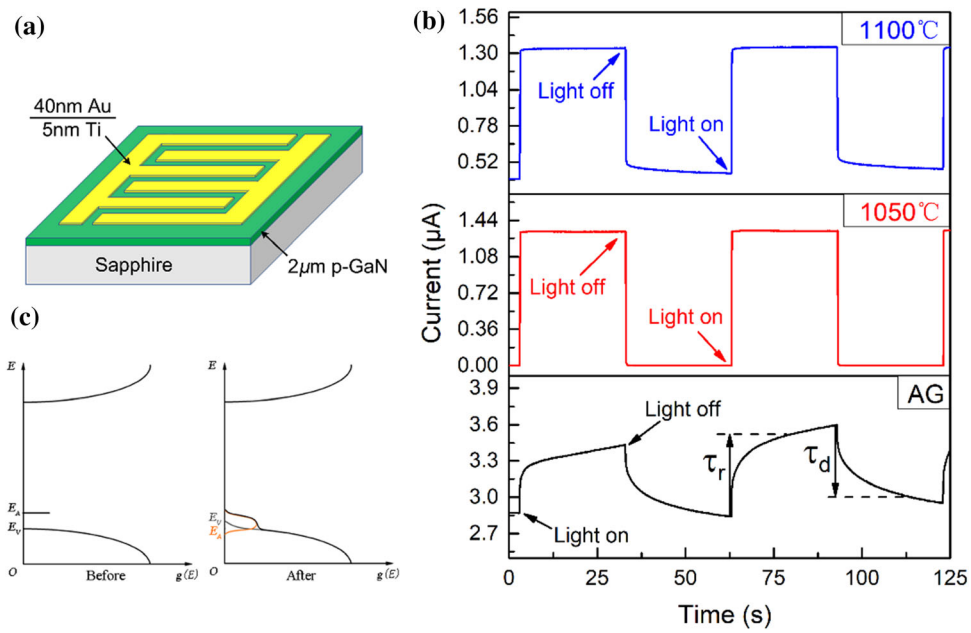

Figure 7 **a** Schematic diagram of photodetector, **b** time response of on/off switching for the photodetector fabricated by the GaN samples before and after the annealing under 405 nm light illumination, **c** band structure of the samples before and after the annealing.

Table 2 The rise time (τ_r), fall time (τ_d), photocurrent (I_{photo}), dark current (I_{dark}) and the on/off ratio (I_{photo}/I_{dark}) of the photodetectors fabricated by the GaN films before and after the annealing

Sample	τ_r (s)	τ_d (s)	I_{photo}(μA)	I_{dark}(μA)	I_{photo}/I_{dark}
S_1[a]	19.11	18.95	3.60	2.95	1.22
S_2[b]	0.078	0.155	1.33	6.71×10^{-4}	2.0×10^3
S_3[c]	0.297	0.590	1.34	0.47	2.85

[a–c] corresponds to photodetectors of as-grown GaN, 1050 °C-annealed GaN and 1100 °C-annealed GaN

have the potential to make photodetectors. To explore the effect of the annealing temperature, a comparison is made between the two photodetectors prepared by the annealed GaN films. It can be observed from Table 2, the S_2 photodetector presents much better photoelectric conversion performance (e.g., higher on/off ratio and faster response speed) than the S_3 detector.

Owing to the 1100 °C-annealed GaN film with the badly damaged surface, the 1050 °C-annealed sample has lower interface trap state density generated by the defects at the interface between GaN and metal, which can increase the height of the Schottky barrier. The high Schottky barrier can present electrons from overcoming the barrier to generate leakage current [42], meaning that the dark current and on/off ratio of the S_2 photodetector are much lower and higher than the S_3, respectively. Furthermore, the response speed is mainly affected by the carrier drift process in the film as well as the recombination and generation of electron–hole pairs [6]. Therefore, the increase of τ_r and τ_d of the S_3 photodetector should be attributed to deterioration of the crystal at 1100 °C, leading to destruction of the periodic potential field. The destruction results in the enhancement of scattering [35, 43, 44]. These factors indicate that the 1100 °C-annealed sample has lower carrier mobility than the 1050 °C-annealed sample.

Conclusion

Due to the chemical inertness of p-type GaN, it cannot be applied to fabricate a porous structure by wet etching. We report a novel method to fabricate porous p-GaN films by the thermal annealing in N_2 atmosphere. Compared with the as-grown sample, the annealed samples have high responsibility at the visible light regions, and the porous GaN obtained at 1050 °C exhibits faster carrier mobility, higher response speed and similar visible light transmittance. Our studies will enable the rational control of porous structure toward the fabrication of GaN-based devices having the desired optoelectronic properties.

Acknowledgements

This work was supported by the National Natural Science Foundation of China [Grant number 61874067]; the Key Technology Research and Development Program of Shandong [Grant number 2018GGX102024]; and the Natural Science Foundation of Shandong Province [Grant number ZR2019MF042].

References

[1] Yu R, Wang G, Shao Y, Wu Y, Wang S, Lian G, Zhang B, Hu H, Liu L, Zhang L, Hao X (2019) From bulk to porous GaN crystal: precise structural control and its application in ultraviolet photodetectors. J Mater Chem C 7(45):14116–14122. https://doi.org/10.1039/c9tc04820k

[2] Park J, Song KM, Jeon S-R, Baek JH, Ryu S-W (2009) Doping selective lateral electrochemical etching of GaN for chemical lift-off. Appl Phys Lett. https://doi.org/10.1063/1.3153116

[3] Zhang L, Dai Y, Wu Y, Shao Y, Tian Y, Huo Q, Hao X, Shen Y, Hua Z (2014) Epitaxial growth of a self-separated GaN crystal by using a novel high temperature annealing porous template. CrystEngComm 16(38):9063–9068. https://doi.org/10.1039/c4ce01188k

[4] Wang H, Wang W, Yang W, Zhu Y, Lin Z, Li G (2016) Employing Al buffer layer with Al droplets-distributed surface to obtain high-quality and stress-free GaN epitaxial films on Si substrates. J Mater Sci 52(3):1318–1329. https://doi.org/10.1007/s10853-016-0427-1

[5] Zhao C, Yang X, Shen L, Luan C, Liu J, Ma J, Xiao H (2019) Fabrication and properties of wafer-scale nanoporous GaN distributed Bragg reflectors with strong phase-separated InGaN/GaN layers. J Alloy Compd 789:658–663. https://doi.org/10.1016/j.jallcom.2019.03.036

[6] He L, Wang D, Ma X, Feng X, Xiao H, Le Y, Ma J (2020) Fabrication and characterization of ultraviolet detector based on epitaxial Ta-doped Zn2SnO4 films. Opt Mater. https://doi.org/10.1016/j.optmat.2020.110224

[7] Alshahed M, Heuken L, Alomari M, Cora I, Toth L, Pecz B, Wachter C, Bergunde T, Burghartz JN (2018) Low-dispersion, high-voltage, low-leakage GaN HEMTs on native GaN substrates. IEEE Trans Electron Devices 65(7):2939–2947. https://doi.org/10.1109/ted.2018.2832250

[8] Huang S, Zhang Y, Leung B, Yuan G, Wang G, Jiang H, Fan Y, Sun Q, Wang J, Xu K, Han J (2013) Mechanical properties of nanoporous GaN and its application for separation and transfer of GaN thin films. ACS Appl Mater Interfaces 5(21):11074–11079. https://doi.org/10.1021/am4032345

[9] Li XR, Yang XC, Xue HG, Pang H, Xu Q (2020) Metal-organic frameworks as a platform for clean energy applications. EnergyChem 2(2):30. https://doi.org/10.1016/j.enchem.2020.100027

[10] Dai Y, Wu Y, Zhang L, Shao Y, Tian Y, Huo Q, Zhang P, Cao X, Hao X (2014) A novel porous substrate for the growth of high quality GaN crystals by HVPE. RSC Adv 4(66):35106–35111. https://doi.org/10.1039/c4ra04637d

[11] Ghosh D, Devi P, Kumar P (2020) Modified p-GaN microwells with vertically aligned 2D-MoS2 for enhanced photoelectrochemical water splitting. ACS Appl Mater Interfaces 12(12):13797–13804. https://doi.org/10.1021/acsami.9b20969

[12] Lai M, Parish G, Liu Y, Keating AJ, Ieee (2010) Reactive ion etching of porous silicon for MEMS applications. In: Proceedings of 2010 Conference on Optoelectronic and Microelectronic Materials and Devices. In: Conference on optoelectronic and microelectronic materials and devices. pp 169–170

[13] Tserepi A, Tsamis C, Gogolides E, Nassiopoulou AG (2003) Dry etching of porous silicon in high density plasmas. Phys Status Solidi a-Appl Res 197(1):163–167. https://doi.org/10.1002/pssa.200306493

[14] Al Dwayyan AS, Khan MN, Al Salhi AS (2012) Optical characterization of chemically etched nanoporous silicon embedded in Sol-Gel matrix. J Nanomater. https://doi.org/10.1155/2012/713203

[15] Cui J, Xiao H, Cao D, Ji Z, Ma J (2015) Porosity-induced relaxation of strains at different depth of nanoporous GaN studied using the Z-scan of Raman spectroscopy. J Alloy Compd 626:154–157. https://doi.org/10.1016/j.jallcom.2014.11.149

[16] Yang XK, Du XJ, He LN, Wang D, Zhao CC, Liu J, Ma J, Xiao HD (2020) Fabrication and optoelectronic properties of Ga2O3/Eu epitaxial films on nanoporous GaN distributed Bragg reflectors. J Mater Sci 55(19):8231–8240. https://doi.org/10.1007/s10853-020-04600-y

[17] Gao Q, Liu R, Xiao H, Cao D, Liu J, Ma J (2016) Anodic etching of GaN based film with a strong phase-separated InGaN/GaN layer: Mechanism and properties. Appl Surf Sci 387:406–411. https://doi.org/10.1016/j.apsusc.2016.06.081

[18] Cao D, Xiao H, Mao H, Ma H, Gao Q, Liu J, Ma J, Liu X (2015) Electrochemical characteristics of n-type GaN in oxalic acid solution under the pre-breakdown condition. J Alloy Compd 652:200–204. https://doi.org/10.1016/j.jallcom.2015.08.115

[19] Lim WF, Hassan Z, Ahmed NM, Quah HJ (2018) Porous Formation in p-Type Gallium Nitride Films via 50 Hz

Operated Alternating Current-Assisted Photo-Electrochemical Etching in Methanol-Sulfuric Acid Solution. J Electrochem Soc 165(10):H620–H628. https://doi.org/10.1149/2.0591810jes

[20] Bchetnia A, Kemis I, Touré A, Fathallah W, Boufaden T, Jani BE (2008) GaN thermal decomposition in N2AP-MOCVD environment. Semiconduc Sci Technol. https://doi.org/10.1088/0268-1242/23/12/125025

[21] Kim I-H, Park H-S, Park Y-J, Kim T (1998) Formation of V-shaped pits in InGaN/GaN multiquantum wells and bulk InGaN films. Appl Phys Lett 73(12):1634–1636. https://doi.org/10.1063/1.122229

[22] Picard YN, Caldwell JD, Twigg ME, Eddy CR, Mastro MA, Henry RL, Holm RT, Neudeck PG, Trunek AJ, Powell JA (2007) Nondestructive analysis of threading dislocations in GaN by electron channeling contrast imaging. Appl Phys Lett. https://doi.org/10.1063/1.2777151

[23] Heying B, Wu XH, Keller S, Li Y, Kapolnek D, Keller BP, DenBaars SP, Speck JS (1996) Role of threading dislocation structure on the x-ray diffraction peak widths in epitaxial GaN films. Appl Phys Lett 68(5):643–645. https://doi.org/10.1063/1.116495

[24] Zhang Y, Wang J, Su X, Cai D, Xu Y, Wang M, Hu X, Li Z, Jin C, Xu K (2019) Influence of dislocations on the thermal decomposition of GaN. Mater Lett 249:25–28. https://doi.org/10.1016/j.matlet.2019.04.060

[25] Farrer JK, Carter CB (2006) Defect structure in GaN pyramids. J Mater Sci 41(3):779–792. https://doi.org/10.1007/s10853-006-6563-2

[26] Koleske DD, Wickenden AE, Henry RL, Culbertson JC, Twigg ME (2001) GaN decomposition in H-2 and N-2 at MOVPE temperatures and pressures. J Cryst Growth 223(4):466–483. https://doi.org/10.1016/s0022-0248(01)00617-0

[27] Bchetnia A, Kemis I, Toure A, Fathallah W, Boufaden T, El Jani B (2008) GaN thermal decomposition in N-2 AP-MOCVD environment. Semicond Sci Technol 23(12):5. https://doi.org/10.1088/0268-1242/23/12/125025

[28] Davydov VY, Kitaev YE, Goncharuk IN, Tsaregorodtsev AM, Smirnov AN, Lebedev AO, Botnaryk VM, Zhilyaev YV, Smirnov MB, Mirgorodsky AP, Semchinova OK (1998) Phonon spectrum of wurtzite GaN and AlN experiment and theory. J Cryst Growth 189:656–660. https://doi.org/10.1016/s0022-0248(98)00239-5

[29] Al-Heuseen K, Alquran MK (2018) Stress relaxation in porous GaN prepared by UV assisted electrochemical etching. IOP Conf Ser: Mater Sci Eng. https://doi.org/10.1088/1757-899x/305/1/012015

[30] Cao D, Xiao H, Gao Q, Yang X, Luan C, Mao H, Liu J, Liu X (2017) Fabrication and improved photoelectrochemical properties of a transferred GaN-based thin film with InGaN/GaN layers. Nanoscale 9(32):11504–11510. https://doi.org/10.1039/c7nr03622a

[31] Shangguan HQ, Prahl SA, Jacques SL, Casperson LW, Gregory KW (1998) Pressure effects on soft tissues monitored by changes in tissue optical properties. In: Jacques SL, Katzir A (eds) Laser-Tissue Interaction Ix. Proceedings Of, vol 3254. Proceedings of the Society of Photo-Optical Instrumentation Engineers (Spie). pp 366–371. doi:https://doi.org/10.1117/12.308187

[32] Farvacque JL, Bougrioua Z (2003) Carrier mobility versus carrier density in AlxGa1-xN/GaN quantum wells. Phys Rev B 68(3):7. https://doi.org/10.1103/PhysRevB.68.035335

[33] Choi HW, Zhang J, Chua SJ (2001) Dislocation scattering in n-GaN. Mater Sci Semicond Process 4(6):567–570. https://doi.org/10.1016/s1369-8001(02)00019-7

[34] Hakim MO, Islam MN (1986) Hall mobility and carrier scattering mechanism in thin SnO2 film. J Bangladesh Acad Sci 10(2):171–175

[35] Egan RJ, Chin VWL, Tansley TL (1994) Dislocation scattering effects on electron-mobility in INASSB. J Appl Phys 75(5):2473–2476. https://doi.org/10.1063/1.356244

[36] Hu T-J, Cui X-Y, Li X-F, Wang J-S, Yang J-H, Gao C-X (2015) In Situ Electrical Resistivity and Hall Effect Measurement of beta-HgS under High Pressure. Chinese Phys Lett. https://doi.org/10.1088/0256-307x/32/1/016402

[37] Grabow LC, Uhlrich JJ, Kuech TF, Mavrikakis M (2009) Effectiveness of in situ NH3 annealing treatments for the removal of oxygen from GaN surfaces. Surf Sci 603(2):387–399. https://doi.org/10.1016/j.susc.2008.11.029

[38] Majid A, Ahmad N, Rizwan M, Khan Salah U-D, Ali FAA, Zhu J (2017) Effects of Mn Ion implantation on XPS spectroscopy of GaN thin films. J Electron Mater 47(2):1555–1559. https://doi.org/10.1007/s11664-017-5955-1

[39] Grodzicki M, Mazur P, Sabik A (2019) Electronic properties of p-GaN co-doped with Mn by thermal process: surface studies. Surf Sci. https://doi.org/10.1016/j.susc.2019.121460

[40] Godel KC, Steiner U (2016) Thin film synthesis of SbSI micro-crystals for self-powered photodetectors with rapid time response. Nanoscale 8(35):15920–15925. https://doi.org/10.1039/c6nr04759a

[41] Kong Y, Liu L, Xia S, Diao Y, Wang H, Wang M (2016) Optoelectronic properties of Mg doping GaN nanowires. Optical Quantum Electron. https://doi.org/10.1007/s11082-016-0763-z

[42] Lu W, Wang L, Gu S, Aplin DPR, Estrada DM, Yu PKL, Asbeck PM (2011) Analysis of reverse leakage current and breakdown voltage in GaN and InGaN/GaN schottky

barriers. IEEE Trans Electron Devices 58(7):1986–1994. https://doi.org/10.1109/ted.2011.2146254

[43] Makinen J (1992) Positron mobility and trapping in semiconductors. Mater Sci Forum 105–110:369–376

[44] Dzhandieri MS, Tsertsvadze AA (1974) Scattering of carriers by defect complexes screened by free carriers. Soviet Phys Semicond-Ussr 8(4):499–500